Published in final edited form as:
Eur J Neurosci. 2012 August ; 36(3): 2302–2310. doi:10.1111/j.1460-9568.2012.08159.x.

The development, distribution and density of the PMCA2 calcium pump in rat cochlear hair cells

Qingguo Chen[1,2,*], **Shanthini Mahendrasingam**[3,*], **Jacqueline A. Tickle**[3], **Carole M. Hackney**[4], **David N. Furness**[3], and **Robert Fettiplace**[2]

[1]Department of Otolaryngology-Head and Neck Surgery, Tongji Hospital, Tongji Medical, College, Huazhong University of Science and Technology, Wuhan, China

[2]Department of Neuroscience, University of Wisconsin Medical School, Madison, WI 53706

[3]Institute for Science and Technology in Medicine, School of Life Sciences, Keele University, Keele, Staffs ST5 5BG, UK

[4]Department of Biomedical Science, University of Sheffield, Sheffield, S10 2TN, UK

Abstract

Calcium is tightly regulated in cochlear outer hair cells (OHCs). It enters mainly via mechanotransducer (MT) channels and is extruded by the PMCA2 isoform of the plasma membrane calcium ATPase, mutations in which cause hearing loss. To assess how pump expression matches the demands of Ca^{2+} homeostasis, the distribution of PMCA2 at different cochlear locations during development was quantified using immunofluorescence and post-embedding immunogold labeling. The PMCA2 isoform was confined to stereociliary bundles, first appearing at the base of the cochlea around post-natal day 0 (P0) followed by the middle and then the apex by P3, and was unchanged after P8. The developmental appearance matches maturation of the MT channels in rat OHCs. High-resolution immunogold labeling in adult rats showed PMCA2 was distributed along the membranes of all three rows of OHC stereocilia at similar densities and at about a quarter the density in IHC stereocilia. The difference between OHCs and inner hair cells (IHCs) is similar to the ratio of their MT channel resting open probabilities. Gold particle counts revealed no difference in PMCA2 density between low- and high-frequency OHC bundles despite larger MT currents in high-frequency OHCs. The PMCA2 density in OHC stereocilia was determined in low- and high-frequency regions from calibration of immunogold particle counts as $2200/\mu m^2$ from which an extrusion rate of ~200 ions·s^{-1} per pump was inferred. The limited ability of PMCA2 to extrude the Ca^{2+} load through MT channels may constitute a major cause of OHC vulnerability and high-frequency hearing loss.

Keywords

outer hair cell; mechanotransducer channels; adaptation; calcium; voltage-sensitive Ca^{2+} channels

INTRODUCTION

Calcium homeostasis is crucial in the performance and viability of outer hair cells (OHCs) (Beurg et al., 2010), one of two types of sensory receptor cell in the mammalian cochlea. Inner hair cells (IHCs), the main transmission route for auditory signals, synaptically contact

Address correspondence to: Robert Fettiplace, 185 Medical Sciences Building, 1300 University Avenue, Madison, WI, 53706. Tel: 608-262-9320; FAX: 608-265-3500. fettiplace@physiology.wisc.edu.
*Both authors contributed equally to the work.

auditory nerve fiber dendrites (Glowatzki et al 2008) whereas OHCs, by voltage-dependent contractions of their cylindrical soma, are thought to amplify and tune the cochlear response (Dallos et al., 2006; Fettiplace & Hackney 2006). Acoustic stimuli are detected by vibrations of the hair cell stereociliary bundles thereby activating Ca^{2+}-permeable mechanotransducer (MT) channels located at the tips of the stereocilia (Beurg et al., 2006; 2009). Ca^{2+} enters through these MT channels during stimulation and the change in its intracellular concentration is thought to trigger MT channel adaptation (Fettiplace & Ricci 2003) and may also modulate OHC electromotile behavior (Frolenkov et al., 2000). The sole route of Ca^{2+} extrusion is via a plasma membrane calcium ATPase pump, which is present as the PMCA2 isoform in OHC stereocilia (Dumont et al., 2001). A number of mutations of the PMCA2 gene (Atp2b2) have been described, all of which cause some degree of hearing loss or deafness in mice (Street et al., 1998; Kozel et al., 1998; Spiden et al., 2008; Bortolozi et al., 2010). PMCA2 has a restricted neuronal distribution (Stauffer et al., 1995) but the severity of its mutation on hearing is surprising. In humans, mutation of the Atp2b2 gene is also implicated in hearing loss (Schultz et al., 2005; Ficarella et al., 2007). Some mouse mutations are null alleles whereas others exhibit a partial loss of function attributable to reduction in the rate of Ca^{2+} pumping. Those mutations in which the pump is still present but has reduced capacity (e.g., heterozygous *Oblivion, Obl/+*) are associated with progressive hearing loss and OHC apoptosis which begins at the high-frequency base of the cochlea and proceeds towards the low-frequency apex (Spiden et al., 2008). The mechanism of hearing loss stemming from PMCA2 mutation is not well understood. It has been suggested to be partly due to a decrease in endolymphatic Ca^{2+} that weakens tip links (Wood et al., 2004).

To address further the question of Ca^{2+} handling in the hair bundle, we employed quantitative immunofluorescence and post-embedding immunogold labeling to determine how PMCA2 expression matches the differing demands of the hair cells. By calibrating the immunogold labeling we determined the absolute pump density in stereocilia of OHCs with low-and high-characteristic frequencies (CF). Comparison with the Ca^{2+} pump fluxes measured physiologically in low-CF OHCs (Beurg et al 2010) enabled us to derive an important parameter, the extrusion rate per pump. Because of the difficulty of recording from high-CF OHCs at the cochlear base, the Ca^{2+} extrusion rate in these cells is not known. Here, knowledge of the density of PMCA2 pumps at multiple cochlear locations allowed us to infer total extrusion rate in high-CF OHCs and examine the hypothesis that these OHCs may be more susceptible to Ca^{2+} overload.

MATERIALS AND METHODS

Primary antibodies

The primary antibodies were the affinity purified rabbit polyclonal, NR2, an antibody against an N-terminal peptide sequence of PMCA2 (PA1–915 from ThermoFisher Scientific, Pittsburgh, USA and Loughborough, UK, and ab3529 from Abcam, Cambridge UK), and the monoclonal 5F10 antibody (MA3–914 from Af nity Bioreagents, Golden, CO supplied by ThermoFisher Scientific). The NR2 antibodies recognize human and rat PMCA2a and PMCA2b splice variants (Filoteo et al., 1997). It was shown to label stereociliary bundles of rat OHCs (Dumont et al., 2001) and mice OHCs but, in the latter, label disappeared in *deafwaddler*^{2J} (Wood et al 2004), which is a truncated and effectively null mutation in PMCA2. On Western blots of rat organ of Corti lysates, NR2 from Abcam labels two bands at ~127 kDa and 133 kDa probably corresponding to PMCA2a and PMCA2b respectively (Chen et al., 2011). The 5F10 monoclonal antibody recognizes all four PMCA isozymes and has previously been shown to label hair bundles and basolateral membranes of hair cells (Crouch & Schulte, 1995; Yamoah et al., 1998) and a single 140 – 170 kDa band on Western blots of frog saccular hair cells (Yamoah et al., 1998).

Immunofluorescence

The methods of PMCA immunofluorescence staining of cochlear coils were as previously described (Beurg et al., 2010). Sprague–Dawley rats between 0 and 21 days postnatal (P0–P21) were anesthetized with isoflurane and killed by decapitation according to methods approved by the Institutional Animal Care and Use Committee of the University of Wisconsin. Cochleae were obtained from at least three pups at each developmental time point. After decapitation, the cochleae were rapidly isolated at 4°C in Hepes buffered salt solution (HBSS) and fixed in 4% paraformaldehyde in phosphate buffer (PB) for 90 min at room temperature. Cochleae from rats older than P10 were decalcified in ethylene diamine tetraacetic acid (EDTA) (pH 7.2–7.4) for 3–4 days at 4°C. After unpeeling cochlear bone and removing the stria vascularis and tectorial membrane, the cochlear coils were isolated, divided into apical, middle and basal turns, and treated with 0.5% Triton X-100 for 30 min at room temperature and rinsed in phosphate-buffered saline (PBS). The cochlear coils were then immersed in 10 per cent normal goat serum (Invitrogen Life Sciences) for 1h at room temperature to block non-specific labeling and incubated overnight at 4°C with primary antibody (either NR2 or 5F10 at dilutions of 1:400). The blocking solution was used instead of primary antibody in the control groups. After rinsing in PBS, specimens were incubated with Alexa Fluor 488 goat anti-rabbit IgG antibody (1:400; Invitrogen Life Sciences, CA) or Alexa Fluor 488 goat anti-mouse IgG antibody (1:400; Jackson ImmunoResearch Laboratories, West Grove, PA) diluted in blocking solution for 2h at room temperature, rinsed in PBS, incubated with Alexa Fluor 568 phalloidin (1:200; Invitrogen Life Sciences) for 60 min at room temperature and rinsed in PBS. The preparations were mounted in Prolong Antifade medium (Invitrogen Life Sciences, CA) with cover slips and viewed under a 60X (Nikon ELWD Plan uor, NA = 1.4) oil-immersion objective using a Bio-Rad MRC-1024ES laser scanning microscope system (Bio Rad, Hemel Hempstead, UK) operating in confocal mode. Immunostaining for PMCA2 and for all four isoforms was analyzed in the apical, middle, and basal turns of cochlear coils at each time point. The time points were: P0, P2, P4, P6, P8, P10, P13, and P21 for the NR2 antibody and P2, P6, P9, and P14 for the 5F10 antibody. The three cochlear locations were at approximate fractional distances (distance along the cochlea from its basal end normalized to its total length, which is about 10 mm) of 0.8, 0.5 and 0.2 and corresponded to CFs of 4, 14 and 30 kHz (Müller, 1991). The fluorescence intensity was measured from confocal images taken under identical conditions and equal photomultiplier settings using ImageJ software (National Institute of Health, Bethesda, MD) or Adobe Photoshop (version 8.0, San Jose, CA). In each preparation, fifteen OHCs (from all three rows) and five IHCs were randomly selected to measure the fluorescence intensity through hair cell bundle and hair cell body and the averaged fluorescence intensity was calculated.

Immunogold labeling

Fixation and LR-white resin embedding—Cochlear segments were isolated from three Sprague-Dawley rats (P26) using procedures approved by the Animal Care Committee at the University of Wisconsin and in accordance with the UK Animals Scientific Procedures (Act of 1986). Two animals were given an overdose of sodium pentobarbitone (IP; Pentoject, 100 mg/kg) (Animalcare Ltd, York, UK), decapitated, the bullae opened and each cochlea was fixed by perfusion with 4% paraformaldehyde and 0.1% glutaraldehyde in 0.1M phosphate buffer (PB, pH 7.4) through the round window and a small hole in the apex, then immersed in the same fixative for 2h. A third animal was fixed transcardially for 1 min with a vascular flush of PBS containing 5% dextran or heparin (7.2 U/min) and 0.15% procaine HCl and then for 10 min with 4% PFA and 0.1% GTA in (pH 7.4), followed by further fixation by perfusion of the same fixative via small holes made in the cochlear base and apex, followed by immersion in the same fixative for 2 h at room temperature (Hackney et al., 2005). After washing in 0.1M PB, the bony walls of the cochleae were removed and

the cochleae were dissected into apical, middle and basal segments. The dissected cochlear segments were then dehydrated in a graded series of ethanols (70%, 80%, 90%, 100%, and dry 100%) for 15 min in each, infiltrated with LR-White resin (Agar Scientific, Stanstead, UK) at room temperature for 24 h and embedded in pure resin polymerized at 50°C for 24h in gelatin capsules. Ultrathin radial sections (100 nm) were cut from apical, middle and basal regions of the cochlea on a Leica Ultracut UCT or a Reichert Ultracut E Microtome and collected on 200-mesh thin bar nickel grids.

Post-embedding immunogold labeling—The grids containing sections were washed in 0.05M Tris buffered saline (TBS, pH 7.4), non-specific labeling blocked with TBS containing 20% goat serum (GS) and 0.2% Tween 20 (TBS-GS-T20) for 30 min at room temperature (~ 20°C). Grids were then incubated overnight at 4°C in one of the primary antibodies (NR2 at dilutions of 1: 50 [20 μg/ml] or 1:200 [5 μg/ml] and 5F10 at a dilution of 1:10) in TBS containing 1% bovine serum albumin (BSA) and 0.2% Tween 20 (TBS-BSA-T20). For a negative control, grids containing sections were incubated in TBS-BSA-T20 without the primary antibody. The sections were then incubated in TBS-BSA-T20 (3 × 10 min), non-specific labeling blocked in TBS-GS-T20 (15 min) and incubated in goat anti-rabbit IgG (British BioCell, Cardiff, UK) conjugated to 10 or 15 nm gold particles diluted 1:20 in TBS-BSA-T20 for 2 h at room temperature. The sections were then washed in TBS followed by distilled water, stained in 2% aqueous uranyl acetate for 20 min and examined using a JEOL-100CX or JEOL JEM 1230 transmission electron microscope operated at an accelerating voltage of 100 kV.

Quantification of PMCA2 using peptide standards—The density of PMCA2 in the stereocilia was quantified by calibrating the immunogold particle counts against known concentrations of the antigen, a procedure previously used for determining the concentration of calcium binding proteins in hair cells (Hackney et al., 2003; 2005). In the current application, stereociliary gold particle counts were calibrated against a gel containing the peptide antigen rather than the entire PMCA2 membrane protein which would not be soluble. The PMCA2 antibody was raised against an N-terminal peptide intracellular sequence of amino acid residues 5–19 (TNSDFYSKNQRNESS) from human PMCA2. Solutions of the 15-residue peptide antigen (ThermoFisher Scientific) were made up at four concentrations of 2, 0.4, 0.08 and 0.016 mg/ml in 10% BSA plus 4% paraformaldehyde in 0.1M PB (pH 7.4) and were solidified into gels by the addition of 0.1% glutaraldehyde. 1–2 mm blocks of each gel standard were dehydrated and embedded in LR White resin in the same way as the rat cochlear segments to provide peptide standards. Ultrathin sections of the peptide standard gels were cut onto nickel grids and immunogold labeled with NR2 antibody (ThermoFisher, diluted 1:200 (5 μg/ml) or Abcam diluted 1:50) and 10 nm gold conjugated goat anti-rabbit IgG diluted 1:20, both in TBS-BSA-T20 under the same conditions and in parallel with radial sections from apical and basal locations, stained in 2% aqueous uranyl acetate for 20 min and all micrographs were taken at X 30,000.

The stereociliary bundle and gel labeling were compared in two ways: by determining the linear density along the membrane and from the areal density. In the former method, two random micrographs (from each standard gel) of the PMCA2 peptide standard gels were used, and five random lines were drawn on each micrograph. Gold particles were found to lie specifically over dense areas in the images which were assumed to represent areas of precipitated BSA containing the peptide. The density of gold particles/μm length of line was calculated by measuring the lengths of dense regions along the random lines and by counting the number of gold particles on and within the spatial resolution (21 nm) of both sides of the dense regions on each line. The density of gold particles/μm^2 of the peptide standard gels was calculated by using the same micrographs and by placing a grid overlay of equally spaced lines over each micrograph and counting the number of points on the dense

areas to estimate the dense area and counting the gold particles on the dense areas. The average gold particle density in the gels for the four different peptide concentrations was found to increase linearly with concentration, thus ruling out problems that would be caused by saturation. Electron micrographs of OHC stereociliary bundles from apical and basal locations were used to measure the length of the stereociliary membrane and the area of the stereocilia by using the area/perimeter measurement tool in analySIS (Olympus) software. The number of gold particles on the stereociliary membrane and within the spatial resolution (21 nm) of either side of the membrane was counted to determine the density of gold particles/μm length of stereociliary membrane, and the number of gold particles on the stereocilia and within 21 nm external to the stereociliary membrane was counted to calculate the density of gold particles/μm^2. The linear and areal methods gave virtually identical values for the concentration of PMCA2 pumps in the stereocilia (see Results). Having ascertained the gel concentration (in mg/ml) corresponding to the stereociliary label, this was converted into number of molecules (C_P = molecules/μm^3) using a peptide molecular weight of 1777, and the membrane density (molecules/μm^2) was calculated as $[C_P]^{2/3}$.

Freeze Fracture

Freeze fracture replicas of outer hair cells of the human organ of Corti were kindly provided from a previous study by Dan Bagger-Sjöbäck and Berit Engström (Engstrom et al., 1985). These were examined in a JEOL-100CX transmission electron microscope.

Statistics

For the immunofluorescence measurements, values are presented as mean ± standard error of the mean (SEM). Three or more animals were used to construct each data point. Two-way analysis of variance (ANOVA) was used to determine the significance of fluorescence intensity differences during cochlear development. Data were statistically evaluated for significance. The immunogold results are based on three animals. For each cochlear location, multiple fields of view were sampled, and measurements were averaged over the fields of view of both inner and outer hair cells. Multiple fields of view were averaged on a series of micrographs at each location and for each experimental condition. There was no substantive evidence for differences between the three rows of outer hair cells, so the results were pooled across the rows. Values are quoted as mean ± standard error of the mean (SEM) and differences were evaluated with a two-tailed t test or a Wilcoxon signed rank test depending on the distribution of data points or ANOVA.

RESULTS

Immunofluorescence

Immunofluorescence labeling for PMCA2 with the NR2 antibody increased in OHCs over the first postnatal week, appearing first at the base of the cochlea then proceeding towards the apex (Fig. 1A – D), the time difference between the two locations being about two to three days. Half-maximal labeling occurred around P0 at the base and P3 at the apex (Fig. 1D). After P8, the labeling in all three turns reached adult levels and no significant difference between the fluorescence intensity at the three locations was observed. In order to check that a difference in bundle labeling between the locations was not concealed by saturation, fluorescence intensities at P21 were measured at a range of photomultiplier gains and this confirmed that there was no significant difference along the cochlea (Fig. 1E). PMCA2 labeling of the bundles of IHCs was less than that of OHCs (the maximum ratio OHC: IHC bundles was about 5:1) and was also more variable, being visible in some sections especially earlier in development (see Fig. 1B; P6). The reason for the variability is unclear but the relative labeling of the two cell types will be addressed in more depth in the

immunogold experiments. No labeling for PMCA2 was ever observed in the lateral membranes of either OHCs or IHCs (Fig. 1C).

The results illustrated in Fig. 1 provide evidence for only one PMCA isoform. The distribution of all isoforms was examined using the monoclonal 5F10 (Fig. 2A–C) antibody, which recognizes the four PMCA isoforms (Crouch & Schulte, 1995). The acquisition of 5F10 labeling in OHC bundles was very similar to that seen with PMCA2 labeling, appearing first at the base of the cochlea, followed by the middle and then the apex. It reached mature levels by P8 and thereafter little difference was present among three turns (Fig. 2E). These results are consistent with PMCA2 being the sole isoform in OHC bundles (Dumont et al., 2001). As with the PMCA2 antibody, labeling of IHCs bundles with the 5F10 was more variable and most prominent earlier on, where its maximal intensity was about a quarter to a fifth of that in the OHCs (Fig. 2F). In contrast to PMCA2 there was additional label in the lateral membranes of both types of hair cell, reaching a peak around P6 and then declining at older ages in both OHCs and IHCs (Fig. 2G, H). The most likely isoform to account for labeling of the basolateral membrane with the 5F10 antibody is PMCA1 (Dumont et al., 2001). This non-monotonic change in labeling of the basolateral membrane mirrors the development of the voltage-dependent Ca^{2+} current, which reaches a peak at P6 – P8 in IHCs (Johnson et al., 2005; Knirsch et al., 2007) and at about P4 in OHCs (Beurg et al., 2008). Thereafter, the Ca^{2+} current declines to a steady level, which is several-fold larger in IHCs than in OHCs.

The immunofluorescence results demonstrate that hair bundle labeling for PMCA2 increases during the first postnatal week and is fully developed in both apical (low-CF) and basal (high-CF) rat OHCs prior to the onset of hearing around P12. During this period other PMCA isoforms, probably PMCA1 (Dumont et al., 2001; Chen & Fettiplace, unpublished) are present in the OHC lateral membrane but, by the onset of hearing, the intensity of labeling of the lateral membrane is less than a tenth of that in the hair bundle. The results also suggest there is no significant difference (two-way ANOVA; $p > 0.05$) in labeling intensity between OHCs in the low- and high-frequency regions of the cochlea but this conclusion was tested more quantitatively by using immunogold counts in electron microscopic sections which permit sub-cellular resolution.

Post-embedding immunogold

Use of high resolution TEM images allowed a more detailed description of the subcellular distribution of the Ca^{2+} pump; the experiments were performed in adult (P26) rats. PMCA2 labeling was present along the membrane of all three rows of OHC stereocilia (Fig. 3A – C) and a low level of labeling was also observed along the apical membrane as reported by Grati et al., (2006). The results were quantified by counting the number of gold particles in the three different rows and along the stereociliary length. The mean density of gold particles per μm of stereociliary membrane was 0.91 ± 0.04 (± SEM) for the tallest row, 1.03 ± 0.06 (± SEM) for the intermediate row and 1.05 ± 0.06 (± SEM) for the shortest row of stereocilia. No significant difference in labeling was detected between stereociliary rows (one-way ANOVA; $p > 0.05$). Of 91 micrographs assayed for middle turn OHCs, 13 short, 15 intermediate and 32 tall stereocilia were measured (Figure 3C), selecting only stereocilia whose full height was identifiable by their stereociliary tips. The mean heights of the stereocilia were 0.86 μm (range 0.25–1.17 μm) for the shortest row, 1.48 μm (range 1.20–1.73 μm) for the intermediate row and 2.27 μm (range 1.75–2.62 μm) for the tallest row. The distance of each gold particle from the cuticular plate was then measured in relation to the height of the stereociliary tips of each row (Figure 3C). Although label was evident at the tips of the stereocilia and along their entire length, in all three rows gold particle counts were larger along the main shaft compared with the ankle region adjacent to the cuticular plate or tips of the stereocilia (Fig. 3C).

Sparser labeling but with a similar distribution was seen in IHC stereocilia (Fig. 4). Two sets of counts from one animal made in the basal region were: 0.6 ± 0.1 gold particles/μm in OHCs (n = 13) and 0.16 ± 0.1 particles/μm in IHCs (n = 4) (± SEM) giving a ratio of 3.75; and 1.53 ± 0.10 gold particles/μm in OHCs (n = 8) and 0.41 ± 0.1 particles/μm in IHCs (n = 4) (± SEM) giving a ratio of 3.8. In both counts the difference between OHCs and IHCs was significant (Wilcoxon signed rank test; $p < 0.05$). The measurements indicate a four-fold greater PMCA2 labeling in OHCs than IHCs and confirm the immunofluorescence results which gave up to a five-fold difference between the stereociliary bundles of the two hair cell types.

Immunogold low-CF/high-CF comparison

The MT current in high-CF OHCs at the base of the cochlea is several-fold larger than that in low-CF OHCs at the apex, the current magnitude increasing systematically with CF (Beurg et al., 2006; Johnson et al., 2011). This gradient implies that the hair bundle Ca^{2+} load increase significantly along the cochlea, it is therefore important to determine whether there are any concomitant changes in PMCA2 density. Labeling for PMCA2 in OHC bundles was quantified at low-CF and high-CF cochlear locations and gold particle counts indicated no major difference between the two locations. Gold particle counts were expressed both as a linear density along the plasma membrane and as an areal density and, to minimize steric hindrance, in most experiments 10 nm gold particles were used. Values for three P26 rats, using both linear and areal counts are given in Table 1. The ratio of gold particle densities between the high-CF and low-CF regions using the linear counts was 1.07 ± 0.2, 1.02 ± 0.29 and 1.31 ± 0.24 (± SEM) in the three animals respectively. In all cases, therefore, stereociliary labeling was slightly higher in the high-CF than in the low-CF region, but the differences were not significant in any of the animals (Wilcoxon signed rank test; $P > 0.05$). Pooling the two methods in the three animals gave a mean high-CF/low-CF ratio of 1.19 ± 0.19 (± SEM). These results suggest there is no difference in PMCA2 pump density between the low-frequency apical and high-frequency basal OHCs.

The quantification was extended to obtain the absolute pump density by calibrating the immunogold labeling against labeling of a gel containing a known concentration of the peptide antigen. Use of the peptide antigen rather than the insoluble PMCA2 membrane protein assumes that the peptide alone adopts a similar conformation to the same sequence in the protein and thus will bind the antibody with the same efficiency as the native protein. Since the peptide is hydrophilic and originates from near the free intracellular amino terminus of the pump, this assumption seems under the circumstances to be reasonable. The peptide was made up at a range of concentrations into gels that were fixed and sectioned and the sections were then treated identically to the tissue sections. The ratio of gold particle densities in the OHC bundles and in the gel (Fig. 5) was then used to infer the PMCA2 concentration in the bundle.

The gold particle densities were determined in two ways, as a count along the stereociliary membrane (linear) and as a count over the area of the stereocilia (areal). In one animal, the linear gold particle density on the OHC stereociliary membrane was 1.31 ±0.07/μm (n = 23; low-CF region) and 1.02 ±0.08/μm (n = 23; high-CF region) (± SEM) using the NR2 antibody from ThermoFisher. Comparison with the gel gave a concentration of 0.33 ± 0.02 mg/ml (± SEM) in low-CF OHCs and 0.24 ± 0.02 mg/ml (± SEM) in high-CF OHCs. If the areal density was used on the same micrographs, the gold particle density in the OHC bundle was 37.6 ± 2.3/μm^2 (n = 23; low-CF) and 38.3 ± 1.9/μm^2 (n = 23; high-CF) (± SEM). The corresponding peptide concentrations were 0.45 ± 0.04 mg/ml (± SEM) in low-CF OHCs and 0.45 ± 0.03 mg/ml (± SEM) in high-CF OHCs. Similar measurements were made employing both linear and areal counts with the NR2 antibody from Abcam. These gave peptide concentrations in the OHC stereocilia of 0.16 ± 0.01 mg/ml and 0.14 ± 0.01

mg/ml (± SEM) for the low-CF and high-CF regions respectively with linear counts and of 0.30 ± 0.02 mg/ml and 0.40 ± 0.02 mg/ml (± SEM) for the low-CF and high-CF using areal counts. For both antibodies, the values for low and high frequency regions were very similar irrespective of the method used and again indicated no substantial difference between the two cochlear locations. Combining the four values at each position irrespective of technique or antibody gave peptide concentrations of 0.31 ± 0.11 mg/ml (± SEM) in the low-frequency region and 0.31 ± 0.14 mg/ml (± SEM) in the high-frequency region. These values represent the concentrations of the peptide in the gel the immunolabeling of which is equivalent to the PMCA2 in the hair bundle. They can be converted into PMCA2 densities by calculating the molecular concentration (molecules/μm^3) using the molecular weight of the peptide and then taking the two-thirds power to give the areal density in molecules/μm^2 (see Methods). Taking the means of the two methods and antibody sources gives equivalent PMCA2 densities of 2197 ± 542 molecules/μm^2 (± SEM) in the low-CF region and 2159 ± 708 molecules/μm^2 (± SEM) in the high-CF region. These results further reinforce the conclusion that there is no difference in PMCA2 density in the stereocilia of low-CF and high-CF OHCs.

Freeze fracture

Correlations of this high pump density were observed in freeze fractures of human OHC stereocilia (Fig. 6) prepared for a previous study (Engström et al., 1985). The inner leaflet face of the membrane of the stereociliary shaft was adorned with a roughly uniform array of particles at a density of 2000 – 2500 particles/μm^2 (mean = 2355/μm^2). A measurement in the ankle region gave a lower density of 813/μm^2. The size of the particles, the majority of which are ~8 nm in diameter, is consistent with the dimensions of the inner surface of the sarcoplasmic reticulum Ca^{2+}-ATPase predicted from x-ray diffraction, no x-ray diffraction data yet being available for the PMCA (Toyoshima, 2008; Brini & Carafoli, 2009). If the particles do indeed primarily represent PMCA2 molecules, their density is consistent with quantification of the immunolabeling and further indicates that the pump exists largely in a monomeric form, not multimeric as has been suggested (Sackett & Kosk-Kosicka, 1996).

DISCUSSION

Developmental appearance and distribution of PMCA2

We have used both immunofluorescence and post-embedding immunogold labeling to quantify the development and distribution of the PMCA2 isoform in rat cochlear hair cells. Several conclusions of functional relevance can be drawn from the measurements. Firstly, labeling of the OHC stereociliary bundles with the PMCA2 isoform exhibited a base to apex development similar to many other properties that change during cochlear maturation. The high-CF OHCs at the cochlear base attained maximal labeling at P2, preceding the apex by about two to three days, and thereafter there was no change into adulthood (P21). This time course is very similar to the appearance of the MT channels in rat OHCs, where all cells are transducing by P2 in the base and P5 in the apex (Waguespack et al., 2007). Other properties of transduction, including Ca^{2+}-driven adaptation, matured over the same time frame. The close correspondence in the time courses suggests either that the two properties are co-regulated or else they are causally linked as, for example, might occur if the elevation of intracellular Ca^{2+} by influx through newly-acquired MT channels provides a signal for incorporation of Ca^{2+} pumps into the stereociliary membrane.

A second conclusion concerns the stereociliary distribution of pumps deduced form immunogold labeling. For OHCs, PMCA2 labeling of the bundles showed all three rows of stereocilia were equally labeled approximately evenly along their shafts. Similar results have been reported (Apicella et al., 1997) and were evident in previous immunofluorescence

labeling (Grati et al., 2006). The equal distribution of label contrasts with the observation that the MT channels are present only in the middle and short stereociliary rows (Beurg et al., 2009). However, this discrepancy might merely reflect utilization of the entire membrane area of the bundle given the high packing density of the pumps. Furthermore, since the pumps operate on a slow time scale of seconds (e.g., Beurg et al., 2010), and the PMCA2 has a high Ca^{2+} affinity (0.1 μM; Elwess et al., 1997), they would still be in a position to extrude Ca^{2+} that had diffused back into the tallest row from the other stereociliary rows (Beurg et al., 2009). A similar pattern of labeling was evident on the IHC stereocilia, though the gold particle density was a quarter of that seen in the OHCs. A possible explanation for this difference in pump density between the two types of hair cell is that, in the steady state, the fraction of MT channels open at rest (and therefore the resting Ca^{2+} load) is smaller in IHCs than in OHCs: the resting probability of the channels being open is 0.17 in IHCs and 0.5 in OHCs (Johnson et al., 2011). If this explanation is correct, it implies that the main load on the stereociliary pumps is the resting Ca^{2+} influx via the MT channels.

This conclusion, however, is at odds with the similarity of labeling along the cochlea. Independent observations using immunofluorescence and immunogold indicated that there was no significant difference in pump density between basal and apical OHCs bundles. This result is surprising as the peak amplitude of the MT current in OHCs increases several fold between apex and base. The maximum apex-base gradient in the rat cochlea is 4.6, estimated under *in vivo* conditions, including the presence of an endolymphatic potential (Johnson et al., 2011). A more than a four-fold gradient in MT current amplitude from apex to base suggests there will be a substantial increase in the stereociliary Ca^{2+} load in the basal OHCs compared to the apical ones, assuming the MT channels at the two locations have the same Ca^{2+} permeability.

Ca^{2+} homeostasis

We have previously determined the peak Ca^{2+} load as about 7 pA in rat apical OHCs when all the MT channels are open (Beurg et al., 2010); under resting conditions with no stimulation, the probability of opening is ~0.5 (Johnson et al. 2011) which implies there is a continuous resting load of 3.5 pA. This value may be compared with the peak extrusion by the hair bundle PMCA2, which was measured as 18 pA (Beurg et al., 2010). Therefore at the apex, a good safety margin exists and all the Ca^{2+} entering though the MT channels can be pumped out. However, extrapolation of these results to basal OHCs indicates that, because of an increase in the amplitude of the MT currents, the standing Ca^{2+} load will be 16 pA and the peak load will be twice that. Clearly if the pumps in the high-CF basal OHCs perform at the same rate, they will barely extrude even the resting load, let alone the extra amount entering during acoustic stimulation. Furthermore, because of the three-fold decrease in stereociliary height from 6 μm at the apex to 2 μm at the base (Roth & Bruns, 1992) and the concomitant reduction in stereociliary diameter (0.25 μm to 0.15 μm; Johnson et al., 2011; Fig. 4B), the volume of the hair bundle compartment will be much reduced as will the total membrane area of the hair bundle. As a consequence, the Ca^{2+} concentration in this restricted compartment due to Ca^{2+} influx through the MT channels will be at least four-fold larger thus causing saturation of the cytoplasmic Ca^{2+} buffers. We propose that the propensity for Ca^{2+} overload in the basal high-CF OHCs may be a contributory factor to their greater vulnerability, especially if the pump efficiency is reduced, as in some PMCA2 mutations where OHC loss progresses from the high-CF base to the low-CF apex (Spiden et al., 2008; Bortolozzi et al., 2010).

PMCA2 density and turnover rate

A new finding in the present work was a value of ~2200/μm^2 for the OHC stereociliary density of PMCA2 pumps which are predominantly present as the PMCA2 w/a splice variant (Hill et al., 2006; Chen et al., 2011). Since the maximum pump rate (18 pA), inferred from the electrogenic pump current in apical OHCs (Beurg et al. 2010), is known, this allows calculation of the rate of a single PMCA2 monomer as 200 Ca^{2+} ions·s^{-1} (at room temperature), assuming an area of 250/μm^2 for the stereociliary membrane of rat apical OHCs based on reported dimensions (Roth & Bruns, 1992). The calculation assumes that the PMCA2 is predominantly in monomeric form in the stereociliary membrane. However, if some or all of the pumps were dimeric (Vorherr et al., 1991; Sackett & Kosk-Kosicka, 1996), the inferred pump density may be up to two-fold larger (due to possible steric hindrance, each 10 nm-immunogold particle may label only one of the PMCA2 molecules in each dimer) and the pumping rate would be correspondingly smaller. The inferred pumping rate is large for P-type ATPases. For example, the single molecule turnover rate for the Na-K ATPase pump has been measured as 60 ions·s^{-1}, also at room temperature (Friedrich et al., 1996). A range of 5 to 100 ions·s^{-1} (Kubitscheck et al., 1995) was inferred (as here from the total extrusion rate and the pump density) for the Ca^{2+} ATPase pump in erythrocytes (mainly PMCA4) and the present estimate is outside this range. A density of ~2000/μm^2 and a pump rate of 120 ions·s^{-1} was estimated for the same isoform in bullfrog stereocilia (Yamoah et al., 1998). PMCA2 is regarded as a fast neuronal Ca^{2+} pump (Caride et al., 2001) and the high single-molecule turnover rate of ~200/s inferred here accords with this notion. PMCA2 is located at sites of high Ca^{2+} turnover, particularly dendritic spines of both Purkinje cells and hippocampal pyramidal cells (Burette et al., 2009; 2010) where its role in Ca^{2+} regulation may be crucial for expression of long term potentiation (Simons et al., 2009). In the spines, as in the dimensionally similar stereocilia, the high pumping rate may be critical for maintaining Ca^{2+} homeostasis in a small sub-cellular compartment subject to a large Ca^{2+} load.

Acknowledgments

This work was supported by grants from the National Institutes on Deafness and other Communication Disorders (RO1 DC01362) and from the UW Steenbock Foundation to RF and from AoHL (the RNID) to DNF. Qingguo Chen was supported by grant 2009616042 from the Chinese Scholarship Council. We thank Dan Bagger-Sjöbäck and Berit Engström for the freeze fracture replicas of organ of Corti and Bechara Kachar for helpful advice.

Abbreviations

BSA	bovine serum albumen
CF	characteristic frequency
EDTA	ethylene diamine tetra-acetic acid
HBSS	Hank's buffered saline solution
IHC	inner hair cell
MT	mechanotransducer
OHC	outer hair cell
P	postnatal day
PB	phosphate buffer
PBS	phosphate buffered saline
PFA	paraformaldehyde

PMCA	plasma membrane calcium ATPase
TBS-BSA-T20	Tris-buffered saline containing 1% bovine serum albumin and 0.2% Tween 20
TBS-GS-T20	Tris-buffered saline containing 20% goat serum and 0.2% Tween 20

References

Apicella S, Chen S, Bing R, Penniston JT, Llinas R, Hillman DE. Plasmalemmal ATPase calcium pump localizes to inner and outer hair bundles. Neuroscience. 1997; 79:1145–1151. [PubMed: 9219973]

Beurg M, Evans MG, Hackney CM, Fettiplace R. A large-conductance calcium-selective mechanotransducer channel in mammalian cochlear hair cells. J Neurosci. 2006; 26:10992–11000. [PubMed: 17065441]

Beurg M, Safieddine S, Roux I, Bouleau Y, Petit C, Dulon D. Calcium- and otoferlin-dependent exocytosis by immature outer hair cells. J Neurosci. 2008; 28:1798–803. [PubMed: 18287496]

Beurg M, Fettiplace R, Nam JH, Ricci AJ. Localization of inner hair cell mechano-transducer channels using high-speed calcium imaging. Nature Neurosci. 2009; 12:553–558. [PubMed: 19330002]

Beurg M, Nam JH, Chen Q, Fettiplace R. Calcium balance and mechano-transduction in rat cochlear hair cells. J Neurophysiol. 2010; 104:18–34. [PubMed: 20427623]

Bortolozzi M, Brini M, Parkinson N, Crispino G, Scimemi P, De Siati RD, Di Leva F, Parker A, Ortolano S, Arslan E, Brown SD, Carafoli E, Mammano F. The novel PMCA2 pump mutation Tommy impairs cytosolic calcium clearance in hair cells and links to deafness in mice. J Biol Chem. 2010; 285:37693–703. [PubMed: 20826782]

Brini M, Carafoli E. Calcium pumps in health and disease. Physiol Rev. 2009; 89:1341–78. [PubMed: 19789383]

Burette AC, Strehler EE, Weinberg RJ. “Fast” plasma membrane calcium pump PMCA2a concentrates in GABAergic terminals in the adult rat brain. J Comp Neurol. 2009; 512:500–13. [PubMed: 19025983]

Burette AC, Strehler EE, Weinberg RJ. A plasma membrane Ca^{2+} ATPase isoform at the postsynaptic density. Neuroscience. 2010; 169:987–93. [PubMed: 20678993]

Caride AJ, Filoteo AG, Penheiter AR, Pászty K, Enyedi A, Penniston JT. Delayed activation of the plasma membrane calcium pump by a sudden increase in Ca^{2+}: fast pumps reside in fast cells. Cell Calcium. 2001; 30:49–57. [PubMed: 11396987]

Chen Q, Chu H, Wu X, Cui Y, Chen J, Li J, Zhou L, Xiong H, Wang Y, Li Z. The expression of plasma membrane Ca(2+)-ATPase isoform 2 and its splice variants at sites A and C in the neonatal rat cochlea. Int J Pediatr Otorhinolaryngol. 2011; 75:196–201. [PubMed: 21094535]

Crouch JJ, Schulte BA. Expression of plasma membrane Ca-ATPase in the adult and developing gerbil cochlea. Hearing Res. 1995; 92:112–119.

Dallos P, Zheng J, Cheatham MA. Prestin and the cochlear amplifier. J Physiol. 2006; 576:37–42. [PubMed: 16873410]

Dumont RA, Lins U, Filoteo AG, Penniston JT, Kachar B, Gillespie PG. Plasma membrane Ca^{2+}-ATPase isoform 2a is the PMCA of hair bundles. J Neurosci. 2001; 21:5066–5078. [PubMed: 11438582]

Elwess NL, Filoteo AG, Enyedi Á, Penniston JT. Plasma membrane Ca^{2+} pump isoforms 2a and 2b are unusually responsive to calmodulin and Ca^{2+} J Biol Chem. 1997; 272:17981–17986. [PubMed: 9218424]

Engström B, Hoffstedt M, Bagger-Sjöbäck D. A technique for freeze-fracturing of the organ of Corti. Acta Otolaryngol Suppl. 1985; 423:36–42. [PubMed: 3864346]

Fettiplace R, Hackney CM. The sensory and motor roles of auditory hair cells. Nat Rev Neurosci. 2006; 7:19–29. [PubMed: 16371947]

Fettiplace R, Ricci AJ. Adaptation in auditory hair cells. Curr Opin Neurobiol. 2003; 13:446–451. [PubMed: 12965292]

Ficarella R, Di Leva F, Bortolozzi M, Ortolano S, Donaudy F, Petrillo M, Melchionda S, Lelli A, Domi T, Fedrizzi L, Lim D, Shull GE, Gasparini P, Brini M, Mammano F, Carafoli E. A functional study of plasma-membrane calcium-pump isoform 2 mutants causing digenic deafness. Proc Natl Acad Sci USA. 2007; 104:1516–1521. [PubMed: 17234811]

Filoteo AG, Elwess NL, Enyedi A, Caride A, Aung HH, Penniston JT. Plasma membrane Ca^{2+} pump in rat brain. Patterns of alternative splices seen by isoform-specific antibodies. J Biol Chem. 1997; 272:23741–7. [PubMed: 9295318]

Friedrich T, Bamberg E, Nagel G. Na+, K+-ATPase Pump Currents in Giant Excised Patches Activated by an ATP Concentration Jump. Biophys J. 1996; 71:2486–2500S. [PubMed: 8913588]

Frolenkov GI, Mammano F, Belyantseva IA, Coling D, Kachar B. Two distinct Ca(2+)-dependent signaling pathways regulate the motor output of cochlear outer hair cells. J Neurosci. 2000; 20:5940–8. [PubMed: 10934241]

Glowatzki E, Grant L, Fuchs P. Hair cell afferent synapses. Curr Opin Neurobiol. 2008; 18:389–395. [PubMed: 18824101]

Grati M, Schneider ME, Lipkow K, Strehler EE, Wenthold RJ, Kachar B. Rapid turnover of stereocilia membrane proteins: evidence from the trafficking and mobility of plasma membrane Ca^{2+}-ATPase 2. J Neurosci. 2006; 26:6386–6395. [PubMed: 16763047]

Hackney CM, Mahendrasingam S, Jones EM, Fettiplace R. The distribution of calcium buffering proteins in the turtle cochlea. J Neurosci. 2003; 23:4577–4589. [PubMed: 12805298]

Hackney CM, Mahendrasingam S, Penn A, Fettiplace R. The concentrations of calcium buffering proteins in mammalian cochlear hair cells. J Neurosci. 2005; 25:7867–75. [PubMed: 16120789]

Hill JK, Williams DE, LeMasurier M, Dumont RA, Strehler EE, Gillespie PG. Splice-site A choice targets plasma-membrane Ca2+-ATPase isoform 2 to hair bundles. J Neurosci. 2006; 26:6172–80. [PubMed: 16763025]

Johnson SL, Marcotti W, Kros CJ. Increase in efficiency and reduction in Ca^{2+} dependence of exocytosis during development of mouse inner hair cells. J Physiol. 2005; 563:177–91. [PubMed: 15613377]

Johnson SL, Beurg M, Marcotti WM, Fettiplace R. Prestin-driven cochlear amplification is not limited by the outer hair cell membrane time constant. Neuron. 2011; 70:1143–1154. [PubMed: 21689600]

Knirsch M, Brandt N, Braig C, Kuhn S, Hirt B, Münkner S, Knipper M, Engel J. Persistence of Ca(v)1.3 Ca2+ channels in mature outer hair cells supports outer hair cell afferent signaling. J Neurosci. 2007; 27:6442–51. [PubMed: 17567805]

Kozel PJ, Friedman RA, Erway LC, Yamoah EN, Liu LH, Riddle T, Duffy JJ, Doetschman T, Miller ML, Cardell EL, Shull GE. Balance and hearing deficits in mice with a null mutation in the gene encoding plasma membrane Ca^{2+}-ATPase isoform 2. J Biol Chem. 1998; 273:693–6. [PubMed: 9422719]

Kubitscheck U, Pratsch L, Passow H, Peters R. Calcium pump kinetics determined in single erythrocyte ghosts by microphotolysis and confocal imaging. Biophys J. 1995; 69:30–41. [PubMed: 7669907]

Müller M. Frequency representation in the rat cochlea. Hearing Res. 1991; 51:247–54.

Penheiter AR, Filoteo AG, Croy CL, Penniston JT. Characterization of the deafwaddler mutant of the rat plasma membrane calcium-ATPase 2. Hear Res. 2001; 62:19–28. [PubMed: 11707348]

Roth B, Bruns V. Postnatal development of the rat organ of Corti. II. Hair cell receptors and their supporting elements. Anat Embryol (Berl). 1992; 185:571–581. [PubMed: 1605368]

Sackett DL, Kosk-Kosicka D. The active species of plasma membrane Ca2+-ATPase are a dimer and a monomer–calmodulin complex. J Biol Chem. 1996; 271:9987–91. [PubMed: 8626638]

Schultz JM, Yang Y, Caride AJ, Filoteo AG, Penheiter AR, Lagziel A, Morell RJ, Mohiddin SA, Fananapazir L, Madeo AC, Penniston JT, Griffith AJ. Modification of human hearing loss by plasma-membrane calcium pump PMCA2. N Engl J Med. 2005; 352:1557–64. [PubMed: 15829536]

Simons SB, Escobedo Y, Yasuda R, Dudek SM. Regional differences in hippocampal calcium handling provide a cellular mechanism for limiting plasticity. Proc Natl Acad Sci USA. 2009; 106:14080–4. [PubMed: 19666491]

Stauffer TP, Guerini D, Carafoli E. Tissue distribution of the four gene products of the plasma membrane Ca^{2+} pump. A study using specific antibodies. J Biol Chem. 1995; 270:12184–90. [PubMed: 7538133]

Spiden SL, Bortolozzi M, Di Leva F, Hrabe de Angelis M, Fuchs H, Lim D, Ortolano S, Ingham NJ, Brini M, Carafoli E, Mammano F, Steel KP. The novel mouse mutation *Oblivion* inactivates PMCA2 pump and causes progressive hearing loss. PLoS Genetics. 2008; 4:1–12.

Street VA, McKee-Johnson JW, Fonseca RC, Tempel BL, Noben-Trauth K. Mutations in plasma membrane Ca^{2+}-ATPase gene causes deafness in deafwaddler mice. Nature Genet. 1998; 19:390–394. [PubMed: 9697703]

Toyoshima C. Structural aspects of ion pumping by Ca2+-ATPase of sarcoplasmic reticulum. Arch Biochem Biophys. 2008; 476:3–11. [PubMed: 18455499]

Vorherr T, Kessler T, Hofmann F, Carafoli E. The calmodulin-binding domain mediates the self-association of the plasma membrane Ca^{2+} pump. J Biol Chem. 1991; 266:22–7. [PubMed: 1824694]

Waguespack J, Salles FT, Kachar B, Ricci AJ. Stepwise morphological and functional maturation of mechanotransduction in rat outer hair cells. J Neurosci. 2007; 27:13890–902. [PubMed: 18077701]

Wood JD, Muchinsky SJ, Filoteo AG, Penniston JT, Tempel BL. Low endolymph calcium concentrations in deafwaddler2J mice suggest that PMCA2 contributes to endolymph calcium maintenance. J Assoc Res Otolaryngol. 2004; 5:99–110. [PubMed: 15357414]

Yamoah EN, Lumpkin EA, Dumont RA, Smith PJ, Hudspeth AJ, Gillespie PG. Plasma membrane Ca^{2+}-ATPase extrudes Ca^{2+} from hair cell stereocilia. J Neurosci. 1998; 18:610–24. [PubMed: 9425003]

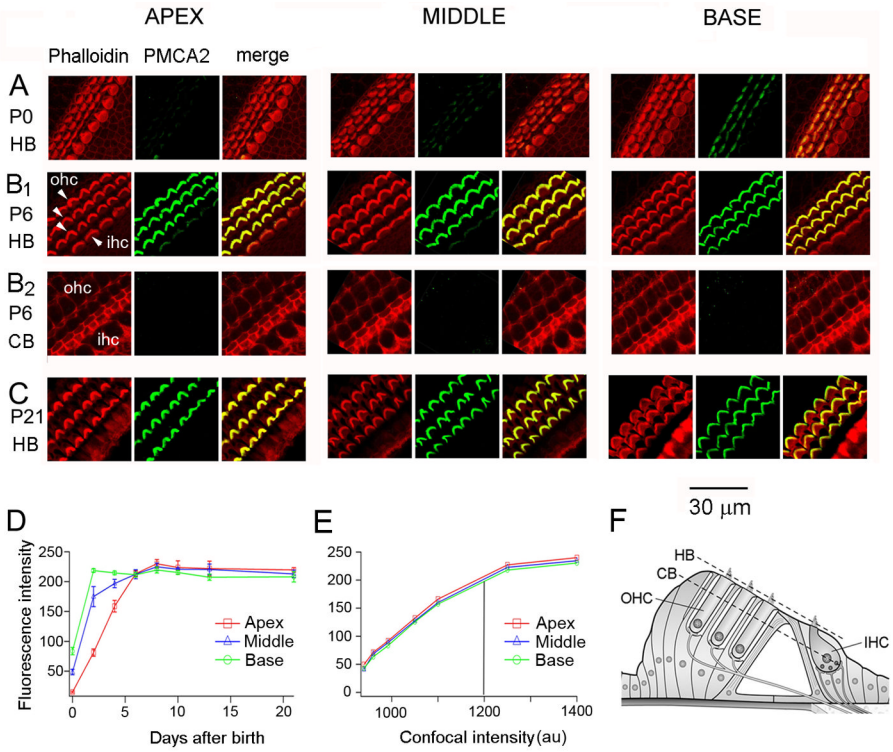

Figure 1.

Developmental appearance of PMCA2 in the rat cochlea. Whole mounts of apical (low-CF), middle (mid-CF) and basal (high-CF) cochlear regions at: A. postnatal day 0 (P0); B1, B2, P6; C, P21. Whole mounts were labeled with the NR2 antibody and with phalloidin to mark the actin and focused on the hair bundle (HB; A, B1, C) and at the cell body (CB; B2). Three rows of outer hair cell bundles (ohc) and one row of inner hair cell bundles (ihc) indicated by arrows in B1 and the corresponding cell bodies in B2. D. Plots of PMCA2 fluorescence intensity in the OHC stereociliary bundle as a function of postnatal age for the three cochlear regions. Each point is the mean ± SEM of 15 OHCs in each of three preparations. E. Plots of the fluorescence intensity in the OHC bundle at P21 as a function of confocal photo-multiplier gain showing no difference between apex, middle and base. F. Schematic diagram of the organ of Corti showing approximate positions of the confocal planes through the hair bundles (HB) and cell bodies (CB) of OHC and IHC.

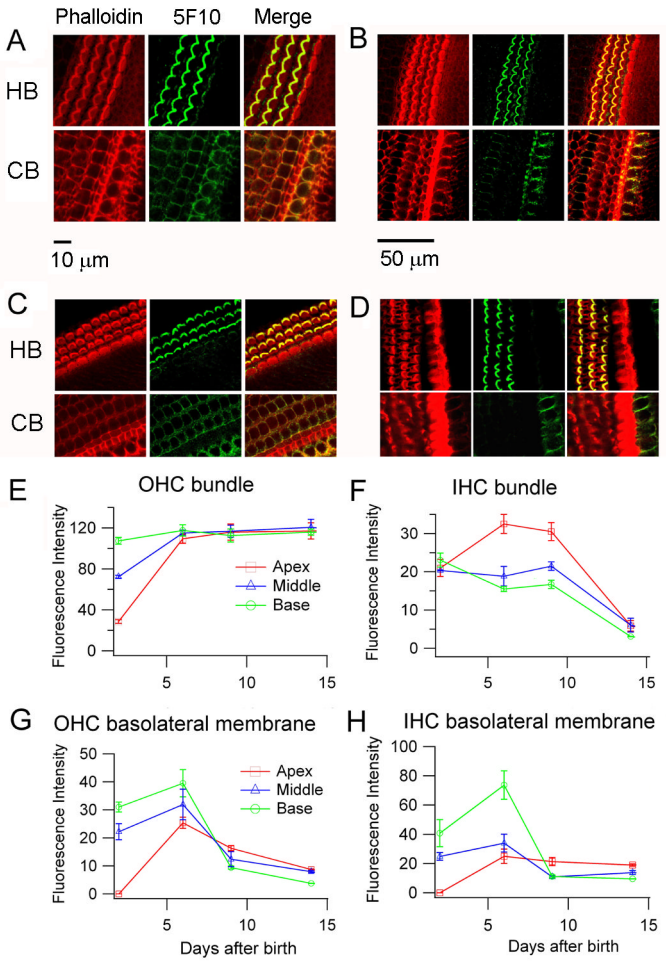

Figure 2.

Developmental appearance of PMCA in the rat cochlea. Whole mounts of apical low-CF cochlear region at P2 (A) P6 (B) P9 (C) and P14 (D). Whole mounts were labeled with the 5F10 monoclonal antibody to all PMCA isoforms and with phalloidin to mark actin and focused on the hair bundle (HB) and cell body (CB); the two confocal planes are shown schematically in Fig. 1F. The 50 μm scale bar applies to B, C and D. Changes in the fluorescence intensities in the OHC bundle (E) and IHC bundle (F) are shown as a function of postnatal age for the apical, middle and basal cochlear regions. Changes in the fluorescence intensities in the OHC (G) and the IHC (H) basolateral membranes are shown as a function of postnatal age for the three cochlear regions. Each point in Fig. 2E and Fig. 2G is the mean ± SEM of 15 OHCs in each of three preparations and in Fig. 2D and Fig. 2H is the mean ± SEM of 5 IHCs in three preparations.

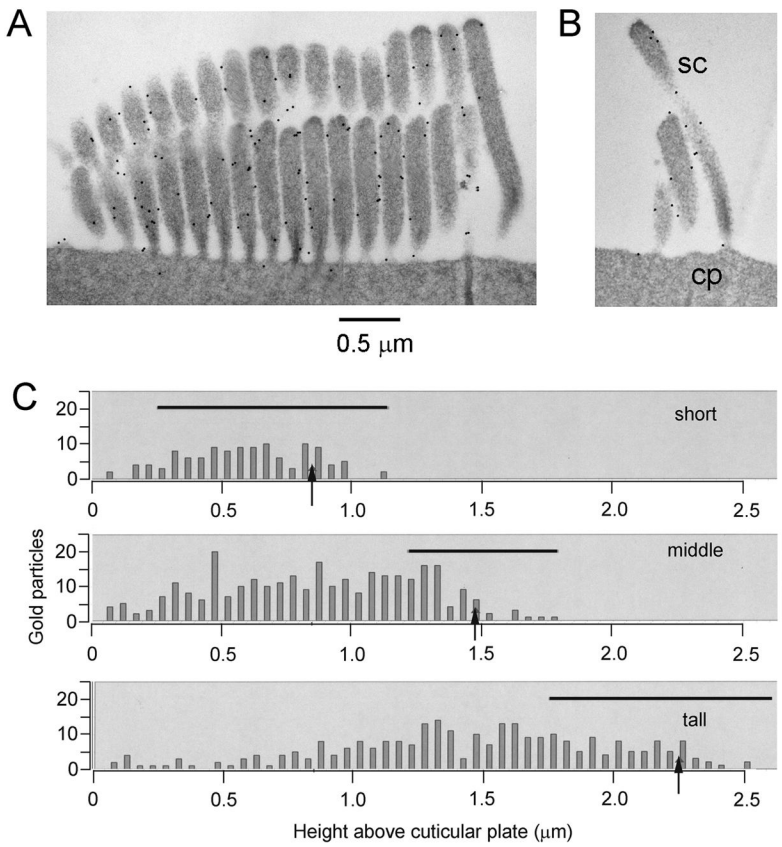

Figure 3.

Post-embedding immunogold labeling for PMCA2 in rat OHCs. A. Transmission electron micrograph of an OHC bundle showing tall and middle row stereocilia labeled with NR2 antibody. Note that labeling is concentrated along the stereociliary membrane of each row with a lower level of labeling found within the actin core. B. Transmission electron micrograph showing labeling in all three stereociliary rows of another OHC; sc, stereocilium; cp, cuticular plate. Scale bar applies to both (A) and (B). C. Histograms showing PMCA2 gold particle labeling in each stereociliary row (short, middle and tall) as a function of the distance from the top of the cuticular plate along the OHC stereociliary membranes. In each histogram, the black line indicates the range of stereociliary heights measurable for each row, the mean height being indicated by the arrow. All OHCs are from the middle region of the cochlea.

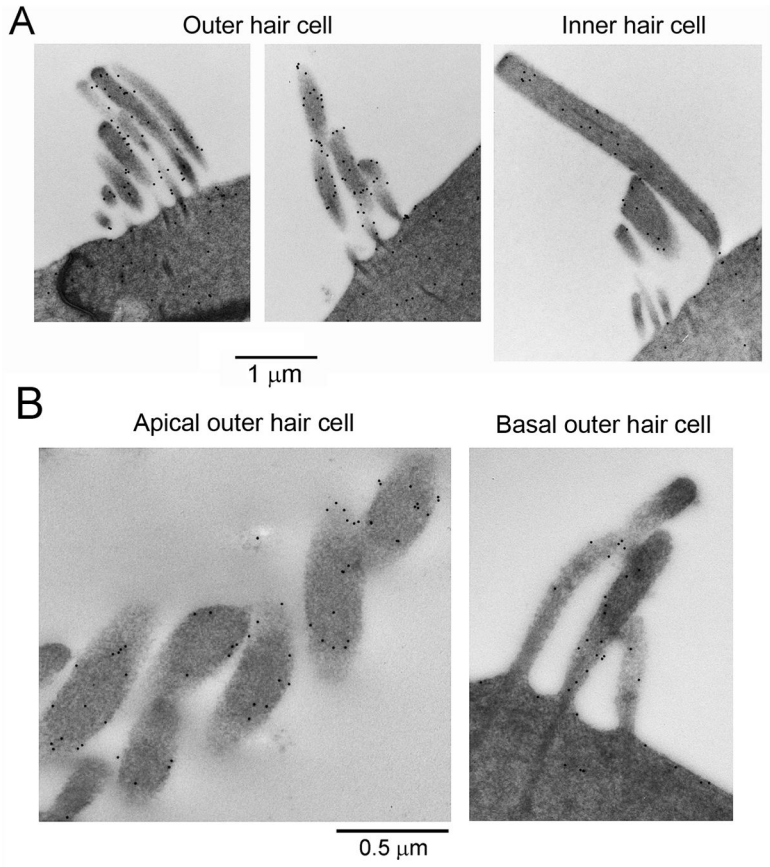

Figure 4.

PMCA2 labeling in rat OHCs and IHCs. A. Radial sections through stereociliary bundles of two OHCs and one IHC from the middle-CF region of the cochlea labeled with NR2 antibody against PMCA2 at the same (1:50) dilution and in the same experiment. Note the heavier labeling of the OHCs than the IHC. The scale bar applies to all images. B. PMCA2 labeling in apical and basal OHCs. Radial sections through stereociliary bundles of OHCs from the apical low- CF (left) and basal high-CF (right) regions of the same rat cochlea labeled with the NR2 antibody (1:50 dilution) in the same experiment. Gold particles are present at roughly the same density in the hair bundles of apical and basal cells. Since the scale bar applies to both micrographs, note the stereocilia at the apex have a larger diameter than those at the base.

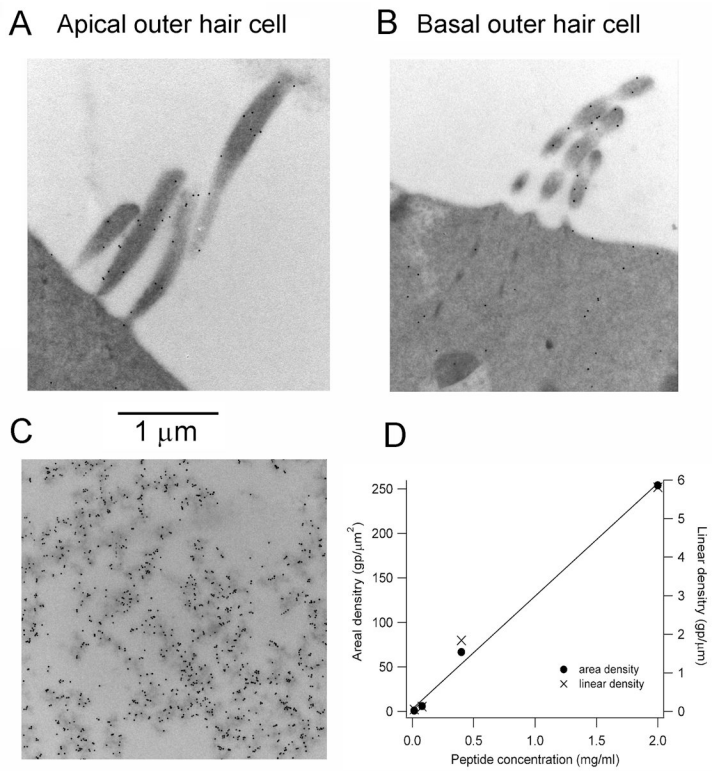

Figure 5.

Calibration of the immunogold labeling. A. Stereociliary bundle of an apical low-CF OHC labeled with the NR2 anti-PMCA2 antibody. B. Stereociliary bundle of a basal high-CF OHC labeled with the same PMCA2 antibody as in (A). C. Labeling with PMCA2 antibody of a section of a gel containing 2 mg/ml of the antigenic peptide against which the antibody was raised (see Methods). Gel and cochlear sections were labeled at the same time with the same antibody dilution. Scale bar applies to all three micrographs. D. Gold particle density in gel, from both areal and linear measurements in gel for four peptide concentrations.

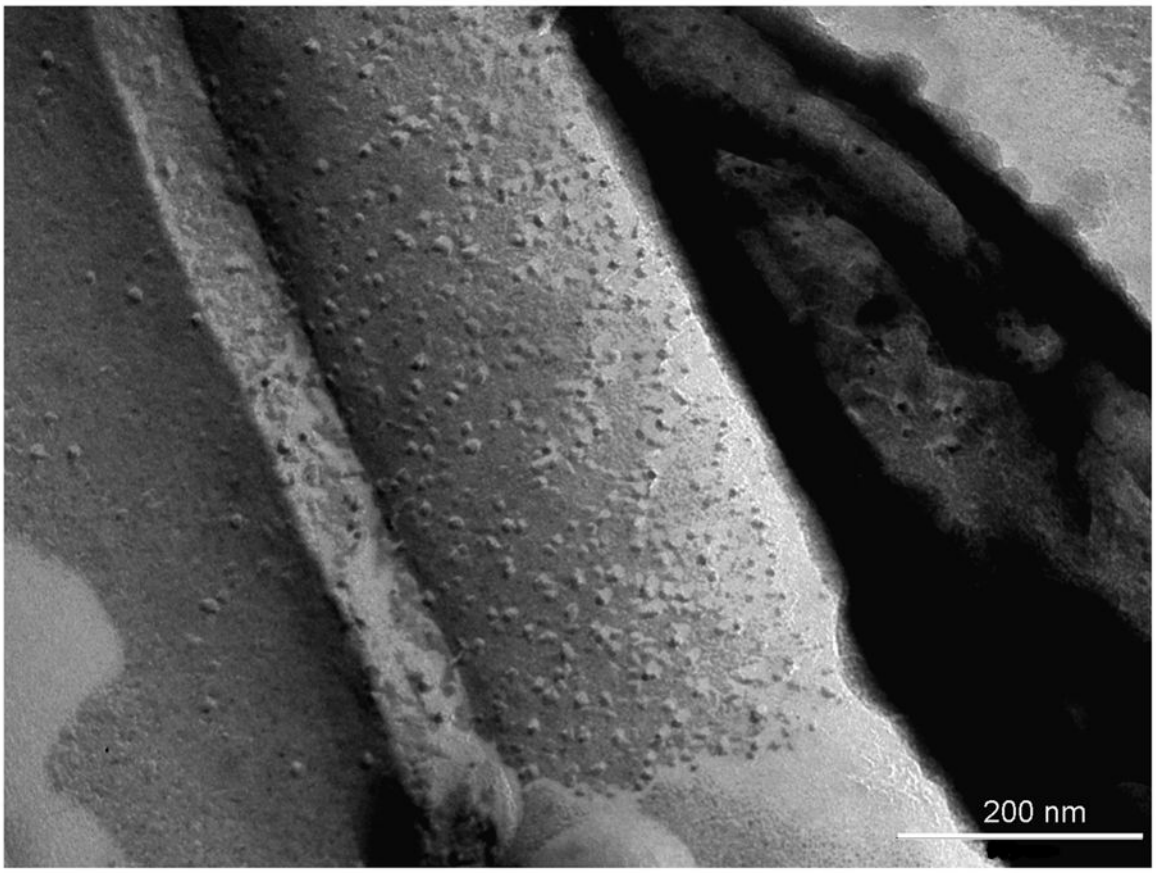

Figure 6.
Freeze fracture of an outer hair cell stereocilium (sc). The fracture plane has gone through the middle of the plasma membrane (between the outer and the inner leaflets of the plasma membrane) to show the inner leaflet over most of the shaft of the stereocilium, with particles clearly visible. The outer leaflet of the membrane is obscuring the particles lower down. Scale bar = 200 nm.

Table 1

PMCA2 immunogold counts in OHC stereociliary bundles

Animal	Method	Base	Apex	Base/apex
R81	linear	1.41 ± 0.17 (27)	1.08 ± 0.07 (14)	1.31 ± 0.24
R81	area	43.9 ± 3.2 (35)	30.5 ± 1.2 (38)	1.44 ± 0.06*
R97	linear	1.54 ± 0.17 (6)	1.51 ± 0.24 (6)	1.02 ± 0.20
R97	area	18.2 ± 2.5 (13)	13.3 ± 1.2 (13)	1.37 ± 0.23
R98	linear	0.16 ± 0.04 (12)	0.15 ± 0.02 (13)	1.07 ± 0.29
R98	area	5.02 ± 1.34 (12)	5.42 ± 1.28 (13)	0.93 ± 0.34

Immunogold particle counts (mean ± SEM, number of micrographs) in stereociliary bundles of OHCs in the high-CF (basal) and low-CF (apical) regions of the cochlea obtained with either linear counts along the membrane or areal counts over the stereocilia. For all except *, there was no significant difference between the apical and basal counts (Wilcoxon signed rank test; $P > 0.05$).